TABLE II

Release of [^{14}C]sucrose from vesicles reconstituted with TOM40 proteins

Results are normalized so that the $^{14}C/^{3}H$ ratios of the incubation mixture would be equal to 1.0. Results of three independent experiments are shown. LDH indicates lactate dehydrogenase.

Addition	Incubation mixture		Isolated vesicles		$^{14}C/^{3}H$
	[^{3}H]Dextran	[^{14}C]Sucrose	[^{3}H]Dextran	[^{14}C]Sucrose	
	cpm		*cpm*		
None	38,200	35,000	5,950	5,230	0.96
Tum40					
3.8 μg	47,900	43,300	9,070	6,640	0.81
38 μg	44,400	40,300	8,110	4,960	0.67
Tom40(ΔN165)					
3.8 μg	43,400	39,500	9,030	7,859	0.97
38 μg	47,600	41,000	9,470	5,650	0.69
Heated 38 μg	52,200	48,400	5,410	4,640	0.92
LDH					
38 μg	45,200	41,000	8,110	7,080	0.96

C-terminal half-segment of rTOM40, like full-size rTOM40, mediates passage of small molecules across the membranes. These properties seem to correspond to the ability of rTOM40 and rTOM40(ΔN165) for sequestration of the MPP-processing site of preprotein within the molecule (see Fig. 3 and Fig. 5).

DISCUSSION

Virtually all the nuclear coded mitochondrial proteins are translocated and sorted into mitochondrial subcompartments via the TOM complex; preproteins transported to the inner compartments are translocated through the TOM channel irrespective of whether they are destined to soluble compartments or to the inner membrane. On the other hand, the outer membrane proteins are sorted by the TOM complex from the proteins destined for the inner compartments and anchored to the lipid bilayer of the outer membrane. As an initial step for understanding the mechanism of this diverse preprotein recognition by the TOM channel, we purified active recombinant rTOM40, and we analyzed the recognition properties using matrix-targeted preproteins.

Purified rTOM40 bound preproteins with high affinity and sequestered the MPP-processing site within the molecule. Furthermore, when reconstituted into liposomes, it exhibited presequence-sensitive cation-selective channel activity. Therefore, recombinant rTOM40 was correctly refolded to attain the functional conformation as the preprotein translocation pore. The CD spectrum of rTOM40 did not exhibit the light-scattering effects caused by aggregated species and revealed a greater than 60% β-sheet structure. This value coincided well with that for recombinant *S. cerevisiae* Tom40 (12), although the CD spectra differed considerably. In contrast, the β-sheet structure content of *N. crassa* Tom40 predicted by CD spectra or IR spectra was markedly lower with a maximum of 31% (10). The α-helical structure of rTOM40 (10%) was half that of *N. crassa* Tom40. The reason for the difference in the secondary structure between *N. crassa* and mammals is not known.

Most importantly, this study demonstrates that the purified membrane embedded C-terminal, half-formed ~170-kDa homo-oligomeric complex with a greater than 60% β-sheet structure and exhibited preprotein-binding properties comparable with those of rTOM40, suggesting that the C-terminal segment constitutes the preprotein conducting pore. Alignment of Tom40 proteins from several organisms revealed that the sequence conservation is higher in the C-terminal pore-forming segment compared with the N-terminal segment (14). Although attempts to measure the presequence-responsive channel activity of rTOM40(ΔN165) electrically were unsuccessful, we could demonstrate that it mediated passage of sucrose across the membrane. This preparation will help analyze the structure of the pore and preprotein recognition mechanisms.

rTOM40(ΔN165) was almost functionally identical with rTOM40 with respect to the preprotein recognition, and both exhibited enriched β-sheet structures, thus the β-barrel structure is responsible for the pore function as is the case for porin (28, 33). The β-structure content of rTOM40(ΔN165) was lower (62%) than that of rTOM40. Because the random coil structure was increased in rTOM40(ΔN165), proper refolding might be disturbed to some extent. The N-terminal 1–165 segment might be required for correct formation or stabilization of the pore structure, and this might be reflected in the decreased affinity of rTOM40(ΔN165) for pSU9-DHFR.

Here we demonstrated that purified recombinant rTOM40 and rTOM40(ΔN165) exhibited virtually identical properties with the TOM core complex (24, 27). They initially bind the preprotein through predominantly electrostatic interactions and partially translocate the preprotein to the salt-resistant *trans*-site that is inaccessible to MPP, probably within the translocation channel. Stabilization of the DHFR moiety by methotrexate inhibited binding of pSU9-DHFR to rTOM40 or rTOM40(ΔN165), suggesting that the partial translocation is accompanied by unfolding of the mature segment, and the activity is restricted to the C-terminal half of rTOM40. These results also indicate that purified rTOM40 as well as rTOM40(ΔN165) contain the salt-sensitive *cis*-binding site. The salt-sensitive binding to the *cis*-site provided by the surface receptors Tom20 and Tom22 is much weaker than that in rTOM40 or rTOM40(ΔN165); *cis*-site binding of the preprotein was almost completely inhibited by 100 mM KCl (22–24). Consistent with this, the K_D values of preproteins for the cytoplasmic domain of import receptors Tom70 or Tom20 as measured by SPR were 10^{-7}–10^{-8} M (34). This affinity difference might facilitate vectorial preprotein transfer from the surface import receptors to the *cis*-binding site of Tom40.

Analysis by SPR revealed that rTOM40 bound pSU9-DHFR with high affinity (in the 10^{-10} M range), and stabilization of the DHFR moiety greatly decreased the affinity. Most interestingly, rTOM40 bound a presequence peptide but with 10^4-fold lower affinity at 3.0×10^{-6} M. These results indicate that the mature portion of the preprotein contributes significantly to the high affinity binding. It should be noted that the rTOM40·pSU9-DHFR complex or rTOM40(ΔN165)·pSU9-DHFR complex, once formed, was resistant to salt treatment, indicating a mode of interaction different from the initial interactions in the latter binding stage or in the *trans*-site binding in the purified molecules. The precise nature of the interaction of the preprotein with the *trans*-binding site remains to be determined. rTOM40 and rTOM40(ΔN165) thus possess

virtually all the preprotein-binding properties characteristic of the TOM holocomplex.

What might be the function of the N-terminal 165-residue segment? rTOM40-(1–165) was expressed in *E. coli* as a soluble form. CD spectra of the purified recombinant rTOM40-(1–165) revealed that it has 49% α-helix, 6% β-sheet, and 45% random structures. The segment consisting of residues 1–65 should span the membrane at least once, although the exact states of membrane disposition of the segment including this and up to 165 residues remains unknown. Recombinant rTOM40-(1–165) bound preprotein with an affinity on the order of 10^{-10} M mainly through hydrophobic interactions; the complex was stable in the presence of 500 mM NaCl.[2] Considering that purified rTOM40 initially binds preproteins by ionic interactions, these results suggest that the 1–165 segment functions in the later stages of preprotein translocation. In *N. crassa* Tom40, segment 41–60 (corresponds to residues 80–98 of rTOM40) is essential for proper assembly/stability of Tom40 in the TOM complex (35). In a recent report, residues 51–60 (correspond to residues 90–98 of rTOM40) and the C-terminal 3 residues (residues 321–323 which correspond to 353–355 of rTOM40) are required for assembly beyond the 250-kDa assembly intermediate of the TOM complex (36). Thus, the N-terminal 1–165 segment might also be involved in the assembly with the TOM components such as Tom22 and small Tom proteins or function as the interface of releasing outer membrane proteins from the import pore into the lipid bilayer. Another possibility is that the N-terminal 1–165 segment is required for coupling the TOM complex with the translocation of inner membrane complex during preprotein transit from the outer membrane to the inner membrane.

Acknowledgments—We thank A. Ito (Kyushu University) for providing us with purified yeast mitochondrial MPP. We also thank T. Ueda (Kyushu University) for help with CD spectrum measurements.

REFERENCES

1. Schatz, G., and Dobberstein, B. (1996) *Science* **271,** 1519–1526
2. Neupert, W. (1997) *Annu. Rev. Biochem.* **66,** 863–917
3. Künkele, K.-P., Heins, S., Dembowski, M., Nargang, F. E., Benz, R., Thieffry, M., Walz, J., Lill, R., Nussberger, S., and Neupert, W. (1998) *Cell* **93,** 1009–1019
4. Pfanner, N., and Geissler, A. (2001) *Nat. Rev. Mol. Cell. Biol.* **2,** 339–349
5. Gabriel, K., Egan, B., and Lithgow, T. (2003) *EMBO J.* **22,** 2380–2386
6. Endo, T., Yamamoto, H., and Esaki, M. (2003) *J. Cell Sci.* **116,** 3259–3267
7. Dekker, P. J. T., Ryan, M. T., Brix, J., Muller, H., Hönlinger, A., and Pfanner, N. (1998) *Mol. Cell. Biol.* **18,** 6515–6524
8. Ahting, U., Thun, C., Hegerl, R., Typke, D., Nargang, F. E., Neupert, W., and Nussberger, S. (1999) *J. Cell Biol.* **147,** 959–968
9. Model, K., Prinz, T., Ruiz, T., Radermacher, M., Krimmer, T., Kühlbrandt, W., Pfanner, N., and Meisinger, C. (2002) *J. Mol. Biol.* **316,** 657–666
10. Ahting, U., Thieffry, M., Engelhardt, H., Hegerl, R., Neupert, W., and Nussberger, S. (2001) *J. Cell Biol.* **153,** 1151–1160
11. Vasiljev, A., Ahting, U., Nargang, F. E., Go, N. E., Habib, S. J., Kozany, C., Panneels, V., Sinning, I., Prokisch, H., Neupert, W., Nussberger, S., and Rapaport, D. (2004) *Mol. Biol. Cell* **15,** 1445–1458
12. Hill, K., Model, K., Ryan, M. T., Dietmeier, K., Martin, F., Wagner, R., and Pfanner, N. (1998) *Nature* **395,** 516–521
13. Esaki, M., Kanamori, T., Nishikawa, S., Shin, I., Schultz, P. G., and Endo, T. (2003) *Nat. Struct. Biol.* **10,** 988–994
14. Suzuki, H., Okazawa, Y., Komiya, T., Saeki, K., Mekada, E., Kitada, S., Ito, A., and Mihara, K. (2000) *J. Biol. Chem.* **275,** 37930–37936
15. Jackson, M. L., and Litman, B. J. (1985) *Biochim. Biophys. Acta* **812,** 369–376
16. Nabekura, J., Omura, T., and Akaike, N. (1996) *J. Neurophysiol.* **76,** 2447–2454
17. Zalman, L. S., Nikaido, H., and Kagawa, Y. (1980) *J. Biol. Chem.* **255,** 1771–1774
18. Reed, J., and Reed, T. A. (1997) *Anal. Biochem.* **254,** 36–40
19. Meisinger, C., Ryan, M. T., Hill, K., Model, K., Lim, J. H., Sickmann, A., Müller, H., Meyer, H. E., Wagner, R., and Pfanner, N. (2001) *Mol. Cell. Biol.* **21,** 2337–2348
20. Komiya, T., Rospert, S., Koehler, C., Looser, R., Schatz, G., and Mihara, K. (1998) *EMBO J.* **17,** 3886–3898
21. Iwahashi, J., Furuya, S., Mihara, K., and Omura, T. (1992) *J. Biochem. (Tokyo)* **111,** 451–455
22. Mayer, A., Neupert, W., and Lill, R. (1995) *Cell* **80,** 127–137
23. Rapaport, D., Neupert, W., and Lill, R. (1997) *J. Biol. Chem.* **272,** 18725–18731
24. Rapaport, D., Mayer, A., Neupert, W., and Lill, R. (1998) *J. Biol. Chem.* **273,** 8806–8813
25. Kanamori, T., Nishikawa, S., Nakai, M., Shin, I., Schultz, P. G., and Endo, T. (1999) *Proc. Natl. Acad. Sci. U. S. A.* **96,** 3634–3639
26. Endo, T., and Kohda, D. (2002) *Biochim. Biophys. Acta* **1592,** 3–14
27. Stan, T., Ahting, U., Dembowski, M., Künkele, K.-P., Nussberger, S., Neupert, W., and Rapaport, D. (2000) *EMBO J.* **19,** 4895–4902
28. Court, D. A., Lill, R., and Neupert, W. (1995) *Can. J. Bot.* **73,** S193–S197
29. Rapaport, D., and Neupert, W. (1999) *J. Cell Biol.* **146,** 321–331
30. Allison, D. S., and Schatz, G. (1986) *Proc. Natl. Acad. Sci. U. S. A.* **83,** 9011–9015
31. Diekert, K., de Kroom, A. I. P., Ahting, U., Niggereyer, B., Neupert, W., Kruijff, B., and Lill, R. (2001) *EMBO J.* **20,** 5626–5635
32. Mihara, K., Blobel, G., and Sato, R. (1982) *Proc. Natl. Acad. Sci. U. S. A.* **79,** 7102–7106
33. Mannella, C., Nuewald, A., and Lawrence, C. (1996) *J. Bioenerg. Biomembr.* **28,** 163–169
34. Iwata, K., and Nakai, M. (1998) *Biochem. Biophys. Res. Commun.* **253,** 648–652
35. Rapaport, D., Taylor, R. D., Käser, M., Langer, T., Neupert, W., and Nargang, F. E. (2001) *Mol. Biol. Cell* **12,** 1189–1198
36. Taylor, R. D., McHale, B. J., and Nargang, F. E. (2003) *J. Biol. Chem.* **278,** 765–775

[2] H. Suzuki, M. Maeda, and K. Mihara, unpublished observations.

J. Anat. (2004) 205, pp135–146

Expression of amyloid precursor protein-like molecule in astroglial cells of the subventricular zone and rostral migratory stream of the adult rat forebrain

Katsunori Yasuoka, Kazuho Hirata, Akio Kuraoka, Jian-wen He and Masaru Kawabuchi

Department of Anatomy and Cell Biology, Graduate School of Medical Sciences, Kyushu University, Fukuoka, Japan

Abstract

In adult mammals, new neurons in the subventricular zone (SVZ) of the lateral ventricle (LV) migrate tangentially through the rostral migratory stream (RMS) to the olfactory bulb (OB), where they mature into local interneurons. Using a monoclonal antibody for the β-amyloid precursor protein (APP) (mAb 22C11), which is specific for the amino-terminal region of the secreted form of APP and recognizes all APP isoforms and APP-related proteins, immunoreactivity was detected in specific subpopulations of cells in the SVZ and RMS of the adult rat forebrain. In the SVZ, APP-like immunoreactivity was detected in the ependymal cells lining the LV and some of the subependymal cells. The latter were regarded as astrocytes, because they were positive for the glial markers, S-100 protein (S-100) and glial fibrillary acidic protein (GFAP). APP-like immunoreactive astrocytes exhibited strong labelling of the perinuclear cytoplasm and often possessed a long, fine process similar to that found with radial glia. The process extended to an APP-like immunoreactive meshwork in the RMS that consisted of cytoplasmic processes of astrocytes forming 'glial tubes'. Double-immunofluorescent labelling with a highly polysialylated neural cell adhesion molecule (PSA-NCAM) confirmed that the APP-like immunoreactive astrocytes in the SVZ and meshwork in the RMS made close contact with PSA-NCAM-immunopositive neuroblasts, suggesting an interaction between APP-containing cells and neuroblasts. This region of the adult brain is a useful *in vivo* model to investigate the role of APP in neurogenesis.

Key words adult neurogenesis; confocal laser scanning microscopy; glial tube; immunohistochemistry; subependymal cell.

Introduction

Mitotic active cell proliferation has been reported in specific regions of the adult mammalian central nervous system (CNS), including the subventricular zone (SVZ) of the lateral ventricle (LV) (reviewed by Alvarez-Buylla & Garcia-Verdugo, 2002), the hippocampal dentate gyrus (Palmer et al. 1997) and the olfactory neuroepithelium (reviewed by Peretto et al. 1999). Attention has increasingly focused upon the SVZ of the LV, because this region is the largest germinal zone of the adult mammalian brain, contains a steady-state population of proliferating cells and harbours neural stem cells that could be used for neuroregenerative therapy (Doetsch & Alvarez-Buylla, 1996; reviewed by Alvarez-Buylla & Garcia-Verdugo, 2002). In addition, a distinct migration pathway called the rostral migratory stream (RMS) has been identified, where neural precursors generated in the anterior horn of the SVZ migrate to the olfactory bulb (OB) and mature into local interneurons (Lois & Alvarez-Buylla, 1994; Lois et al. 1996). Of particular interest is that astrocytes in this region have an immature property that is thought to be involved in the guidance of precursor cells (reviewed by Peretto et al. 1999) or capable of proliferating itself (reviewed by Alvarez-Buylla & Garcia-Verdugo, 2002). The SVZ–RMS–OB system of the forebrain seems

Correspondence
Dr Kazuho Hirata, Department of Anatomy and Cell Biology, Graduate School of Medical Sciences, Kyushu University, Higashi-ku, Maidashi 3-1-1, Fukuoka, 812-8582, Japan. T: +81 92 642 6049; F: +81 92 642 6050; E: hirata@anat1.med.kyushu-u.ac.jp

Accepted for publication *25 June 2004*

to be a useful tool for studying the mechanisms underlying neurogenesis.

Amyloid precursor protein (APP) is an integral cell membrane glycoprotein expressed in a variety of tissues, and is abundant throughout the nervous system (Selkoe, 1994). APP produces the amyloid β protein (Aβ), which is known as the major component of senile plaques found in the brain of patients with Alzheimer's-disease (Goldgaber et al. 1987; Kang et al. 1987; Tanzi et al. 1987). The non-amyloidogenic pathway of APP metabolism involves enzymatic cleavage within the Aβ sequence, and promotes release of the secreted form of APP (sAPP) (Esch et al. 1990; Sisodia et al. 1990). Interestingly, several studies of embryonic (Ohta et al. 1993; Salbaum & Ruddle, 1994) and mutant animals (Mucke et al. 1994; Zheng et al. 1995) have suggested that APP plays a crucial role in neurogenesis. More recent *in vitro* studies, using a yeast expression system, have shown that the amino-terminal region is responsible for the biological activity of sAPP (Ohsawa et al. 1997, 1999; Morimoto et al. 1998a,b), including the enhancement of neurite outgrowth (Ohsawa et al. 1997) and stimulating the proliferation of neural stem cells (Ohsawa et al. 1999). The region is also involved in synapse formation (Morimoto et al. 1998a), although the carboxyl-terminal modulates synaptic activity along with amino-terminal region of sAPP (Morimoto et al. 1998b). Thus the amino-terminal region of sAPP seems to be significantly involved in neurogenesis. A number of studies have localized APP within the nervous system and shown APP expression in a wide range of cell types, including neuronal and non-neuronal cells (Palacios et al. 1992; Banati et al. 1994; Beeson et al. 1994; Ouimet et al. 1994; Chauvet et al. 1997). The considerable variation in the distribution of APP reported by these studies is thought to be partly due to the use of antibodies targeting different regions of the APP molecule (Beeson et al. 1994). Using the monoclonal antibody (mAb) 22C11, which is specific for the amino-terminal region of sAPP, Chauvet et al. (1997) reported APP-like immunoreactivity in immature types of astroglial cells. Although the entire rostrocaudal region of the brain was examined, these authors did not report the distribution of APP in the SVZ–OB system.

In the present study using the mAb 22C11 antibody, APP expression was investigated in the adult rat forebrain, including the SVZ–OB system. APP-like immunoreactivity was detected in ependymal cells and radial glia-like subependymal cells in the SVZ, and a special type of astrocyte forming glial tubes in the RMS.

Materials and methods

Animals and tissue preparation

Adult female Wistar rats weighing 140–160 g (6–8 weeks old) were used. Animals were deeply anaesthetized with diethyl ether and pentobarbital sodium salt (50 mg kg^{-1}) and perfused intracardially with 0.01 M phosphate-buffered saline (PBS) at pH 7.4, followed by a mixture of 4% paraformaldehyde and 0.2% picric acid in 0.1 M phosphate buffer (PB) at pH 7.4. After removal from the skull, the brains were blocked and post-fixed for 3–4 h in 4% paraformaldehyde in 0.1 M PB and immersed overnight in 20% sucrose buffer. They were then frozen with dry-ice-isopentane. The brains were cut either sagittally or frontally into 50-μm-thick serial sections on a cryostat. Sections were collected in 0.02 M potassium phosphate-buffered saline (KPBS).

Antibodies and immunohistochemistry

The immunohistochemical procedure used here has been described previously (He et al. 2000). Briefly, non-specific binding sites were blocked by pre-incubation with 0.1% bovine serum albumin (BSA) in KPBS containing 0.5% Triton X-100 at 4 °C overnight. For immunofluorescent histochemistry of APP, sections were incubated with: (1) the primary antibody, a mouse mAb for the brain Alzheimer precursor protein A4 (APP, 22C11) (Chemicon) at a dilution of 1 : 10 in KPBS at 4 °C for 4 days; (2) the secondary antibody, a biotinylated horse anti-mouse IgG (Vector) 1 : 200 at 4 °C overnight; and (3) fluorescein iso-thiocyanate (FITC)-conjugated streptavidin (1 : 200) for binding to the biotinylated secondary antibodies at 4 °C overnight. Control sections were processed identically and in parallel; however, they were incubated with KPBS instead of the primary antibodies. No labelling of the structures was detected in these controls.

For cellular identification of the immunoreactive elements, a double-immunofluorescence procedure with S-100 protein (S-100) or glial fibrillary acidic protien (GFAP) was performed. Sections were incubated with (1) a mixture of mouse mAb to APP (1 : 10) and rabbit polyclonal antibodies (pAb) to S-100 protein (Nichirei) 1 : 5 or rabbit pAb to GFAP (Research Biochemicals International; RBI) 1 : 100, with (2) a mixture of biotinylated horse anti-mouse IgG (Vector) 1 : 200 and Texas red-conjugated donkey anti-rabbit IgG (Jackson)

Table 1 Primary antibodies used in the immunohistochemical procedures

Antibody (clone)	Source	Dilution	Species
anti-APP (22C11)	Chemicon	1 : 10	Mouse IgG
anti-S-100 protein	Nichirei	1 : 5	Rabbit IgG
anti-GFAP	RBI	1 : 100	Rabbit IgG
anti-vimentin (V9)	Chemicon	1 : 0	Mouse IgG
anti-PSA-NCAM	Dr Seki	1 : 5	Mouse IgM

1 : 200, and then with (3) FITC-conjugated streptavidin (Vector) 1 : 200 for binding to the biotinylated secondary antibodies. To demonstrate the relationship between APP-like-immunolabelled elements and neuroblasts, a double-immunofluorescence procedure for APP and highly polysialylated neural cell adhesion molecule (PSA-NCAM) was used. Sections were incubated with (1) a mixture of the mouse mAb (IgG) to APP and the mouse mAb (IgM) to PSA-NCAM (kindly provided by Dr Seki, Juntendo University, Japan) (1 : 5), with (2) a mixture of biotinylated rabbit anti-mouse IgG (Fc-specific) (Jackson) (1 : 200) and FITC-conjugated goat anti-mouse IgM (μ chain-specific) (Jackson) 1 : 200, and then with (3) Texas red-conjugated streptavidin (Chemicon) 1 : 400 for binding to biotinylated secondary antibodies. The findings of the double-immunofluorescent labelling were compared with those of the single-immunofluorescent labelling, performed using each cellular markers (Table 1) prior to the labelling of the former. No difference was observed in the morphology of the immunolabelled structures between the single and double labelling. The double-labelled sections were mounted on gelatin-coated slides with Vectashield mounting medium (Vector).

To compare APP-like immunolabelled structures with those positive for the immature glial marker, vimentin, a single-immunofluorescence procedure for APP or vimentin was used in two adjacent sections. Serial sections were incubated with (1) the primary antibody, a mouse mAb to anti-APP or mouse mAb to vimentin (V9) (Chemicon) at a dilution of 1 : 10 or 1 : 30 in KPBS, respectively, then with (2) biotinylated horse anti-mouse IgG (1 : 200) as the secondary antibody, and with (3) FITC-conjugated streptavidin (1 : 200) for binding to the biotinylated secondary antibodies.

To identify the nuclei of cells, FITC-labelled sections were counterstained with propidium iodide (PI) using Vectashield mounting medium with PI (Vector).

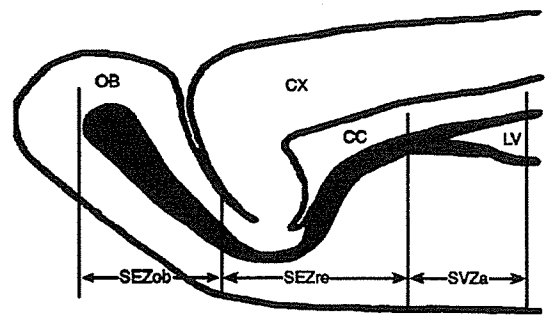

Fig. 1 Schematic diagram of a parasagittal section of the adult rat forebrain and the pathway of migrating precursor cells newly generated in the subventricular zone of the lateral ventricle. Neural precursor cells (black) are generated in the anterior horn of the subventricular zone (SVZa), migrate in a rostral direction (rostral extension of the subependymal zone; SEZre), and eventually reach the olfactory bulb (olfactory bulb portion of the subependymal zone; SEZob), thereby forming the rostral migratory stream (RMS). This schematic representation is also depicted in Figs 2, 3 and 6. LV, lateral ventricle; CX, cerebral cortex; CC, corpus callosum; OB, olfactory bulb.

Confocal laser scanning microscopy

The double-fluorescence-labelled sections were imaged using a confocal laser scanning imaging system (LSM-GB200) attached to a microscope (Olympus). Sections were illuminated by light with an excitation wavelength of 488 nm (argon laser) for FITC, and 568 nm (krypton laser) for Texas red or PI. Single and a series of optical sections were transferred separately to Channel 1 and Channel 2 to avoid crosstalk, and then superimposed. A series of optical sections at 1.5-μm intervals were projected and extended on a single plane 10–20 μm in thickness (volume projection method). Green and red images were acquired simultaneously and are either presented separately (cf. Figs 3 and 4) or as a superimposed image (cf. Figs 2 and 5).

Results

The entire length of the migration pathway for neural precursor cells from the SVZ of the LV to the OB was arbitrarily divided into three regions in a caudal to rostral direction: anterior horn of the SVZ of the LV (SVZa), rostral extension of the subependymal zone (SEZre) and olfactory bulb portion of the subependymal zone (SEZob) (Fig. 1).

In parasagittal sections, the distribution of APP-like-immunoreactive (-ir) structures was clearly observed in conjunction with PI-nuclear staining; the APP-like-ir

components consisted of cells with a prominent cellular configuration in the SVZ (Fig. 2A) and an elaborate network in the RMS (Fig. 2C,D). In the SVZa of the LV, there was intense APP-like immunoreactivity in the perinuclear region of a number of ependymal and subependymal cells (Fig. 2A,B). The subependymal cells often exhibited a similar profile to that of radial glia: rostrally, they extended a long thin process across the wall of the LV into the periventricular parenchyma. These processes were connected with the APP-like-ir network distributed throughout the RMS, including the SEZre (Fig. 2C) and the SEZob (Fig. 2D). The APP-like-ir network was predominant in the SEZre and the most rostral region of the SEZob, due to the dense distribution and more intense immunostaining of the cells. In the most rostral region of the SEZob, the processes of the APP-like-ir network spread out in a fan-shaped manner (Fig. 2D). In some areas of the RMS, a cluster of residual ependymal cells, i.e. a remnant of the olfactory ventricular wall, was occasionally observed as reported by Peretto et al. (1997). These ependymal cells exhibited strong immunoreactivity and were connected with the APP-like-ir network (Fig. 2C).

To identify APP-like-ir cells, double-immunofluorescent labelling for APP and one of the glial markers, S-100 or GFAP, was performed in coronal sections. In the SVZa, APP-like-ir ependymal and subependymal cells were positive for S-100 (Fig. 3A–C) or GFAP (Fig. 3D–F). Furthermore, a comparison of the morphology and distribution of two adjacent coronal (Fig. 3G,H) and parasagittal (Fig. 4A,B) sections revealed that APP-like expression in the SVZa matched that of vimentin, a marker of immature glial cells. Thus, APP-like-ir subependymal cells are probably an immature type of astrocyte. In the core of the SEZre, the APP-like-ir elements were also positive for S-100 (Fig. 5A–C) or GFAP (Fig. 5D–F). APP-like immunoreactivity was mainly detected within the processes, rather than the perinuclear regions, of S-100-ir astrocytes, which form 'glial tubes' in the core of the RMS (Fig. 5A–C). APP-like-ir processes completely overlapped the GFAP-ir processes. APP-like immunoreactivity was slightly stronger in the central region compared with the periphery, whereas GFAP immunoreactivity was somewhat stronger in the periphery (Fig. 5D–F). Thus, APP-like immunoreactivity was only detected in ependymal cells and subependymal astrocytes of the SVZ, and in the astrocytes forming glial tubes in the RMS.

Double-immunofluorescent labelling of coronal sections for APP and PSA-NCAM, a marker of migrating neuroblasts (Bonfanti & Theodosis, 1994), was performed to determine the relationship between APP-like-ir cells and neuroblasts migrating from the SVZ to the OB. In the SVZa, PSA-NCAM-ir elements usually formed a cluster under the layer of APP-like-ir subependymal cells, and were roughly enclosed by loose APP-like-ir networks. PSA-NCAM-ir elements sometimes made contact with APP-like-ir elements (Fig. 6A). In the SEZre, PSA-NCAM-ir elements were more numerous and closely packed in the APP-like-ir networks of glial tubes. In the core of the SEZob, PSA-NCAM-ir elements were also densely packed in APP-like-ir networks (Fig. 6B,C). Thus, PSA-NCAM-ir elements and APP-like-ir networks in the RMS always showed close apposition. In the SEZob, clusters of PSA-NCAM-ir elements were distributed beyond the limits of the core and spread towards the internal granular layer, which exhibited radial migration of neuroblasts (Fig. 6B,D). The cellular localization of PSA-NCAM was confirmed by immunofluorescent labelling of PSA-NCAM and nuclear staining with PI. PSA-NCAM immunoreactivity was observed in cells possessing round and densely stained nuclei, a characteristic of neuroblasts (Fig. 6E).

Discussion

In this study we used the antibody mAb 22C11, which is specific for the amino-terminal region of sAPP (the epitope is localized between residues 66 and 81 of APP) and recognizes all APP isoforms (Hilbich et al. 1993). Slunt et al. (1994) identified cDNA that encodes a 751-amino acid APP-like protein (designated APLP2) in the

Fig. 2 Pseudocolour three-dimensional images reconstructed from a series of 20 sections of immunofluorescent labelling for APP (green) and nuclear staining for PI (red) in the SVZa (A, B), SEZre (C) and SEZob (D) in parasagittal sections of the rat forebrain. (A) In the SVZa, a large number of ependymal and subependymal cells express strong APP-like immunoreactivity in the perinuclear region. Some of the subependymal cells rostrally extend a single, long APP-like-ir process from the cell body. (B) Higher magnification of the white box in A shows APP-like-ir processes of subependymal cells extending across the wall of the LV into the periventricular parenchyma (arrows). (C) In the SEZre, a well-developed APP-like-ir network can be seen in the region of a dense population of PI-stained nuclei in the RMS. Arrow shows that the APP-like-ir network connects with a cluster of APP-like-ir residual ependymal cells. (D) In the SEZob, the APP-like-ir processes spread out in a fan-shaped manner in the most rostral part of the RMS. Scale bars = 10 μm.

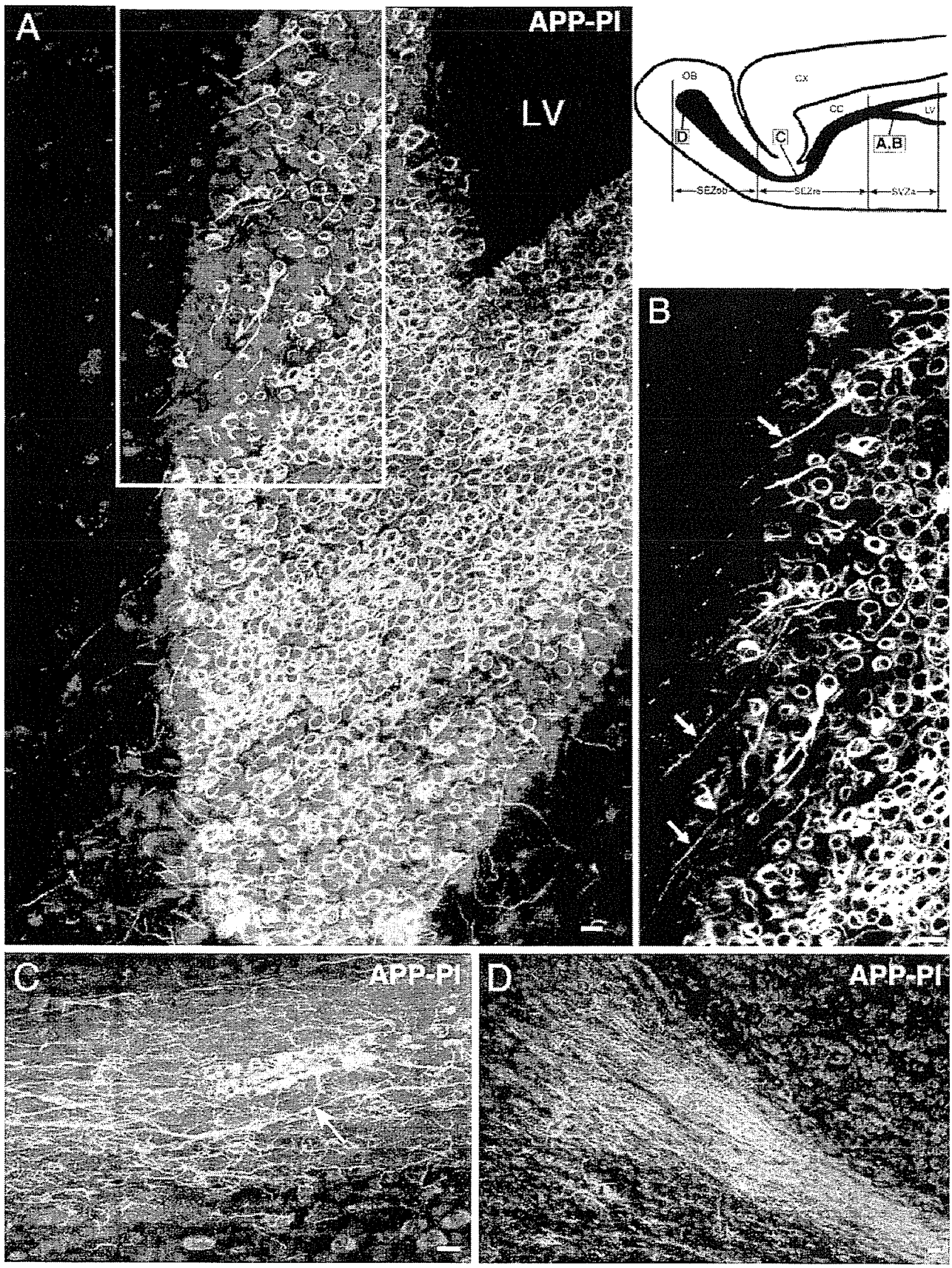

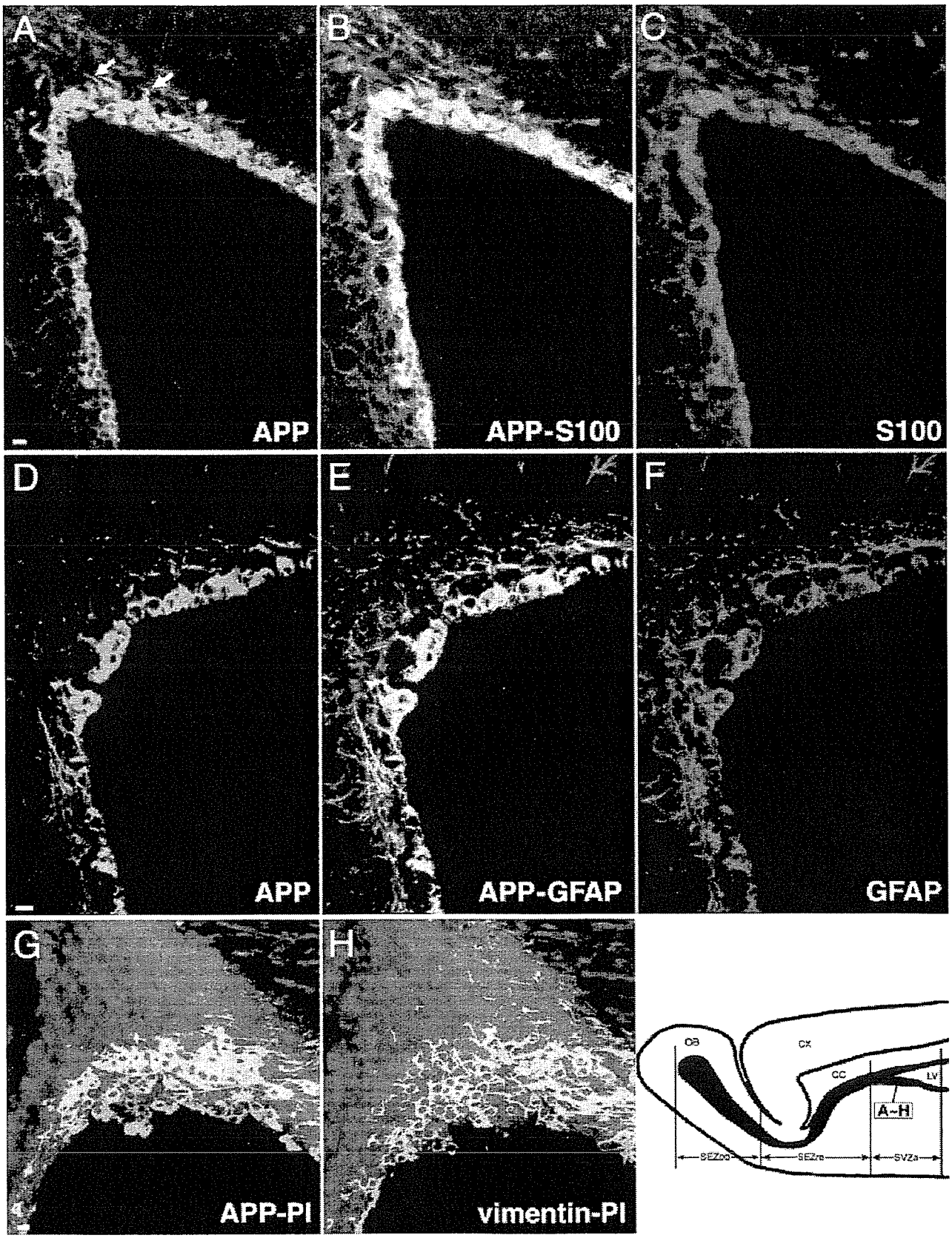

mouse and showed that the mAb 22C11 cross-reacted with mouse APLP2. It cannot be ruled out that the immunoreactivity shown here is not only for APP, but also for APLP, because rat APLP2 has approximately 95% sequence homology with the murine CDEI binding protein (Sandbrink *et al.*, 1994). Hence the immunoreactive site was designated APP-like. In the rat SVZ–OB system, mAb 22C11 immunostaining was detected in specific subpopulations of cells of both the SVZ and the RMS.

In the SVZ, at least two types of APP-like-ir cells were detected: ependymal cells that face the ventricular cavity, and subependymal cells that are located beneath the ependymal cells. The former were immunopositive for S-100 or GFAP, which may include a few tanycytes, i.e. ependymoglial cells, because Doetsch et al. (1997) reported that GFAP-positive tanycytes were occasionally observed in the SVZ. The mAb 22C11 immunostaining in ependymal cells was not confined to this specific region, but detected throughout the lining of the LV (data not shown). The APP-like immunoreactivity of the ependymal cell is consistent with that reported by Chauvet et al. (1997), although they did not describe immunoreactivity in the SVZ. The APP-like-ir subependymal cells were also positive for S100 or GFAP. According to the cellular identification of Doetsch et al. (1997), these cells were regarded as a type of astrocyte. Comparison of two adjacent sections showed that these cells approximately correspond to cells positive for vimentin, which is the major cytoskeletal component in immature glia (Dahl et al. 1981). Furthermore, confocal laser scanning microscopy revealed that APP-like-ir astrocytes often had a long process extending rostrally, and resembled that of radial glia. Although we are not able to state definitely whether these cells are radial glia, APP-like expression in the radial glia-like cells in SVZ of adult rat forebrains is not incompatible with the expression of this molecule in radial glia of the fetal and early postnatal mouse brain (Trapp & Hauer, 1994) and in rat neonatal radial glia-like structures

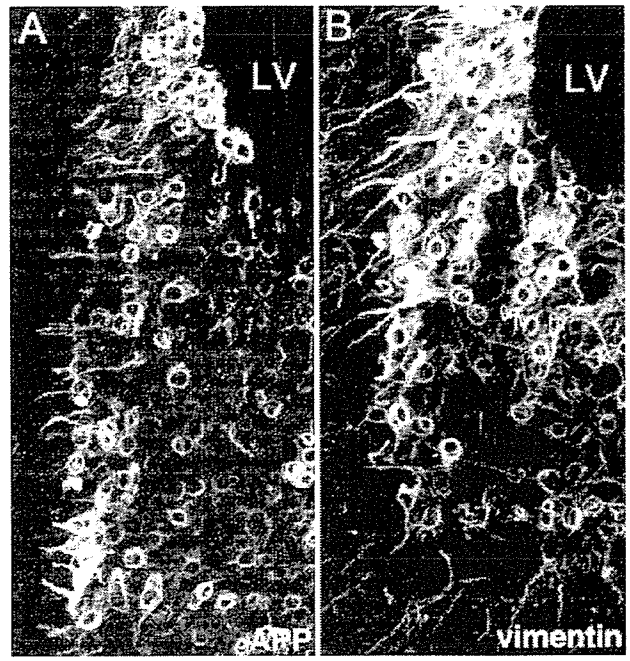

Fig. 4 Greyscale three-dimensional images reconstructed from a series of 20 sections of immunofluorescent labelling for APP (A) and vimentin (B), in two adjacent parasagittal sections of the SVZa. Rostrally directed, long processes of vimentin-ir cells are clearly shown in this parasagittal section (B), whereas the processes of the APP-like-ir cells are apparently shorter, because of being cut in the adjacent section (A).

(Chauvet et al. 1997), the former of which was examined by an mAb raised against the carboxy-terminal region. With regard to the morphology of the astrocytes in the SVZ, there seems to be the difference between the rat and mouse. Astrocytes in the mouse are positive for vimentin (Doetsch & Alvarez-Buylla, 1996), although they exhibited no immunostaining for RC 2 mAb, another marker of radial glia (Gates et al. 1995). However, there is no evidence of a long process, characteristic of radial glia, even in a three-dimensional reconstruction of ultrathin sections (Doetsch & Alvarez-Buylla, 1996; Doetsch et al. 1997). In the mouse SVZ, neuroblasts are thought to traverse a complex network of interconnected pathways formed by astrocytes to enter the

Fig. 3 (A–F) Pseudocolour images of double-immunofluorescent labelling for APP with the glial markers S-100 (A, B, C) and GFAP (D, E, F), in coronal sections of the SVZa. (A–C) Images of FITC-labelled APP-like-ir elements (A) and Texas red-labelled S-100-ir elements (C), and their superimposed image (B), of a single optical section. (D–F) Images of FITC-labelled APP-like-ir elements (D) and Texas red-labelled GFAP-ir elements (F), and their superimposed image (E), of a single optical section. In the SVZa, almost all of the APP-like-ir cells express both S-100 (yellow and yellowish green in B) and GFAP (yellow and yellowish green in E). Note that APP-like expression is confined to the S-100-ir or GFAP-ir elements within the SVZ. Arrows indicate the process extending from the APP-like-ir subependymal cells. (G, H) Pseudocolour three-dimensional images reconstructed from a series of ten optical sections of immunofluorescent labelling for APP (G), and vimentin (H), a marker of immature glial cells, in two adjacent coronal sections of the SVZa. The distribution of the APP-like-ir elements (green and yellow in G) and vimentin-ir elements (green and yellow in H) is very similar. Red indicates PI-stained nuclei. Scale bars = 10 μm.

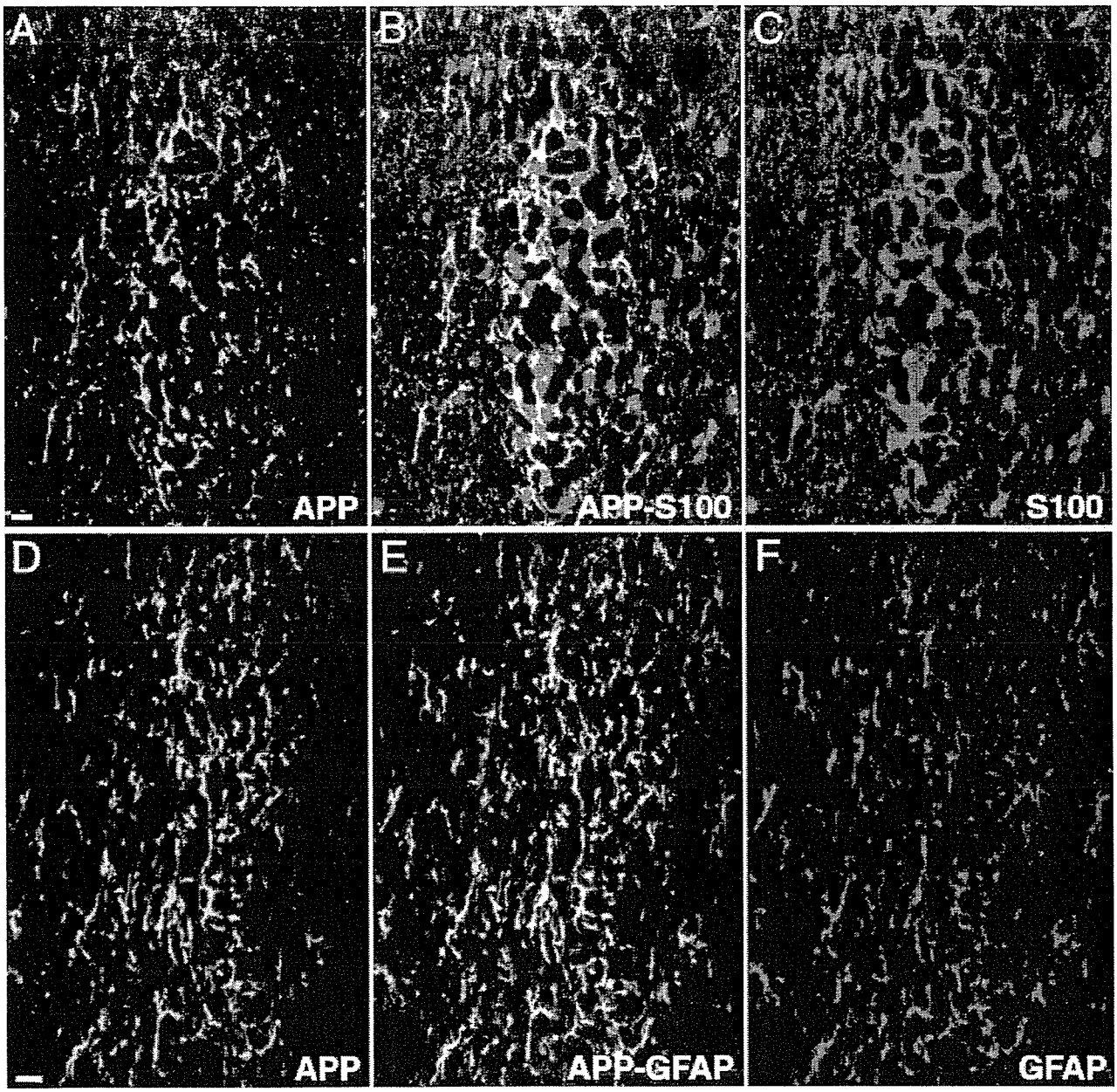

Fig. 5 (A–F) Pseudocolour images of double-immunofluorescent labelling for APP and one for the glial markers S-100 (A–C) or GFAP (D–F), in coronal sections of the SEZre. (A–C) Images of FITC-labelled APP-like-ir elements (A) and Texas red-labelled S-100-ir elements (C), and their superimposed image (B), of a single optical section. In the core of SEZre, APP-like immunoreactivity was co-localized with the processes of S-100-ir astrocytes forming 'glial tubes' (yellow in B). Note that S-100 immunoreactivity occurs throughout the glial cells, including the cytoplasm and the nucleus. (D–F) Images of FITC-labelled APP-like-ir elements (D) and Texas-red-labelled GFAP-ir elements (F), and their superimposed image (E), which were reconstructed from a series of ten optical sections. In the core of the SEZre, all APP-like-ir processes express GFAP (yellow and yellowish green in E). Note that GFAP immunoreactivity is restricted to the cytoplasmic processes, and is distinct from S-100 immunoreactivity (C). Scale bars = 10 μm.

RMS (reviewed by Alvarez-Buylla & Garcia-Verdugo, 2002). In the present study, double immunolabelling with PSA-NCAM showed that PSA-NCAM-positive neuroblasts in the SVZ make contact with the process of APP-like-ir cells. This suggests that the rostral migration of neuroblasts within the SVZ is possibly performed along the shafts of their long process.

In the RMS, the APP-like-ir structure forms an elaborate meshwork. Double immunofluorescent labelling with S-100 or GFAP showed that the APP-like-ir

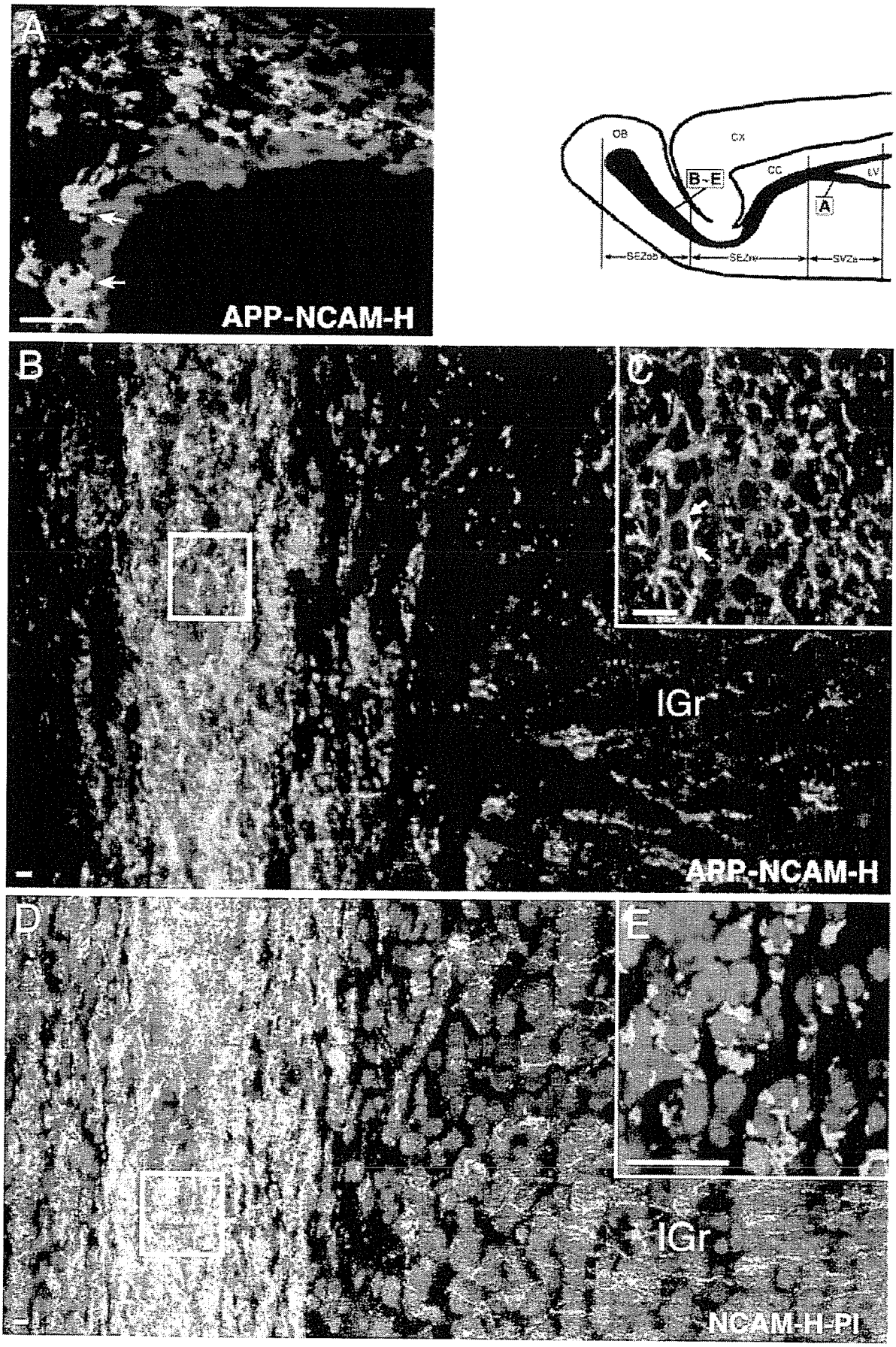

meshwork consisted of astrocyte processes that form tangentially orientated 'glial tubes' (Peretto et al. 1997). These astrocytes also had immature properties, such as the presence of vimentin and glycogen granules in their processes (Peretto et al. 1997). Peretto et al. (1997) suggested that glial tubes could play a role in a unique type of glial guidance that is specifically linked to the peculiar mode of tangential migration of newly generated cells. Here we confirm that PSA-NCAM-ir neuroblasts are densely packed with the APP-like-ir glial tube throughout the RMS. Thus, APP-like-ir astrocytes in the RMS may act as a guide for the migration of neural precursors. However, Wichterle et al. (1997) challenged this assumption from the results of an *in vivo* model of 'chain migration' (Lois et al. 1996). That is, neural precursors could assemble into a chain and migrate along each other without the assistance of ensheathing astrocytes. They assumed that glial cells only play a role in isolating the migrating precursors from the surrounding parenchyma or provide factors for the survival and direction of young migrating neurons. Hence it cannot be determined whether the expression of APP (and possibly APLP2) in the glial tube implicates this protein in the guidance of the neural precursors or in other functions.

The identification of stem cells is crucial for attempts to prepare these cells for therapeutic applications in the future (reviewed by Alvarez-Buylla & Garcia-Verdugo, 2002). Doetsch et al. (1999) revealed that astrocytes in the SVZ are unexpected precursors of new neurons *in vivo* and give rise to cells that grow into multipotent neurospheres *in vitro*. Furthermore, astrocytes in the hippocampus (Seri et al. 2001) and other cell types with astrocytic properties, such as radial glia in the developing neocortex (Malatesta et al. 2000; Miyata et al. 2001; Noctor et al. 2001; Gotz et al. 2002), and Müller cells in the developing retina (reviewed by Fischer & Reh, 2003), have been shown to possess neurogenic potential. Alvarez-Buylla & Garcia-Verdugo (2002) concluded that neural stem cells are contained within the astroglial lineage. By contrast, Johansson et al. (1999) demonstrated that ependymal cells give rise to a rapidly proliferating cell type that generates neurons that migrate to the OB. Thus, the identification of stem cells in the SVZ continues to be disputed, but it is noteworthy that any one of the cell types, i.e. ependymal cells, subependymal astrocytes in the SVZ and astrocytes in the RMS, were positive for mAb 22C11.

The present study has shown that APP-like immunoreactivity was localized to specific subpopulations of cells in the SVZ–OB system of the adult rat forebrain. This region of the adult forebrain could be useful as an *in vivo* model to investigate the role of APP in neurogenesis.

Acknowledgements

We thank Mr Takaaki Kanemaru (Morphology Core, Faculty of Medicine, Kyushu University) for help in preparing the photomicrographs. This work was supported by a Grant-in-Aid for Scientific Research from the Japanese Ministry of Education, Science and Culture (12000210, 12670018).

References

Alvarez-Buylla A, Garcia-Verdugo JM (2002) Neurogenesis in adult subventricular zone. *J. Neurosci.* **22**, 629–634.

Banati RB, Gehrmann J, Kreutzberg GW (1994) Glial beta-amyloid precursor protein: expression in the dentate gyrus after entorhinal cortex lesion. *Neuroreport* **5**, 1359–1361.

Beeson JG, Shelton ER, Chan HW, Gage FH (1994) Differential distribution of amyloid protein precursor immunoreactivity in the rat brain studied by using five different antibodies. *J. Comp. Neurol.* **342**, 78–96.

Bonfanti L, Theodosis DT (1994) Expression of polysialylated

Fig. 6 Relationship between APP-like-ir elements and PSA-NCAM-ir elements in the SVZa (A) and the SEZob (B, C), and the distribution of PSA-NCAM-ir neuronal precursor cells in the SEZob (D, E). (A–C) Pseudocolour images of double-immunofluorescent labelling for APP (red) and PSA-NCAM (green). (A) A single optical section shows that clusters of PSA-NCAM-ir neuroblasts, located under a layer of APP-like-ir ependymal and subependymal cells, are loosely enclosed by APP-like-ir networks. Arrows indicate contact between these elements. (B) A three-dimensional image, reconstructed from a series of ten sections, shows that clusters of PSA-NCAM-ir neuroblasts are more numerous compared with A, and are tightly enclosed by APP-like-ir networks of 'glial tubes' in the core. PSA-NCAM-ir elements spread beyond the limits of the core toward the internal granular layer (IGr), suggesting 'radial migration' of neuroblasts. (C) Higher magnification of a single optical section of the region corresponding to the white box in B shows that two elements are often in close contact. Yellowish green indicates the close apposition (arrows). (D, E) Pseudocolour images of double-immunofluorescent labelling for PSA-NCAM (green and yellow) and nuclear staining with PI (red). (D) Three-dimensional images, reconstructed from a series of ten sections, show that the distribution of PSA-NCAM-ir neuroblasts in the SEZob is clearly indicated by PI nuclear staining. (E) Higher magnification of a single optical section in the white box in D shows that PSA-NCAM immunoreactivity is detected in cells with PI-stained nuclei. Scale bars = 10 μm.

neural cell adhesion molecule by proliferating cells in the subependymal layer of the adult rat, in its rostral extension and in the olfactory bulb. *Neuroscience* **62**, 291–305.

Chauvet N, Apert C, Dumoulin A, Epelbaum J, Alonso G (1997) Mab22C11 antibody to amyloid precursor protein recognizes a protein associated with specific astroglial cells of the rat central nervous system characterized by their capacity to support axonal outgrowth. *J. Comp. Neurol.* **377**, 550–564.

Dahl D, Rueger DC, Bignami A, Weber K, Osborn M (1981) Vimentin, the 57 000 molecular weight protein of fibroblast filaments, is the major cytoskeletal component in immature glia. *Eur. J. Cell Biol.* **24**, 191–196.

Doetsch F, Alvarez-Buylla A (1996) Network of tangential pathways for neuronal migration in adult mammalian brain. *Proc. Natl Acad. Sci. USA* **93**, 14895–14900.

Doetsch F, Garcia-Verdugo JM, Alvarez-Buylla A (1997) Cellular composition and three-dimensional organization of the subventricular germinal zone in the adult mammalian brain. *J. Neurosci.* **17**, 5046–5061.

Doetsch F, Caille I, Lim DA, Garcia-Verdugo JM, Alvarez-Buylla A (1999) Subventricular zone astrocytes are neural stem cells in the adult mammalian brain. *Cell* **97**, 703–716.

Esch FS, Keim PS, Beattie EC, et al. (1990) Cleavage of amyloid beta peptide during constitutive processing of its precursor. *Science* **248**, 1122–1124.

Fischer AJ, Reh T (2003) A. Potential of Müller glia to become neurogenic retinal progenitor cells. *Glia* **43**, 70–76.

Gates MA, Thomas LB, Howard EM, et al. (1995) Cell and molecular analysis of the developing and adult mouse subventricular zone of the cerebral hemispheres. *J. Comp. Neurol.* **361**, 249–266.

Goldgaber D, Lerman MI, McBride OW, Saffiotti U, Gajdusek DC (1987) Characterization and chromosomal localization of a cDNA encoding brain amyloid of Alzheimer's disease. *Science* **235**, 877–880.

Gotz M, Hartfuss E, Malatesta P (2002) Radial glial cells as neuronal precursors: a new perspective on the correlation of morphology and lineage restriction in the developing cerebral cortex of mice. *Brain Res. Bull.* **57**, 777–788.

He JW, Hirata K, Kuraoka A, Kawabuchi M (2000) An improved method for avulsion of lumbar nerve roots as an experimental model of nitric oxide-mediated neuronal degeneration. *Brain Res. Protcol.* **5**, 223–230.

Hilbich C, Monning U, Grund C, Masters CL, Beyreuther K (1993) Amyloid-like properties of peptides flanking the epitope of amyloid precursor protein-specific monoclonal antibody 22C11. *J. Biol. Chem.* **268**, 26571–26577.

Johansson CB, Momma S, Clarke DL, Risling M, Lendahl U, Frisen J (1999) Identification of a neural stem cell in the adult mammalian central nervous system. *Cell* **96**, 25–34.

Kang J, Lemaire HG, Unterbeck A, et al. (1987) The precursor of Alzheimer's disease amyloid A4 protein resembles a cell-surface receptor. *Nature* **325**, 733–736.

Lois C, Alvarez-Buylla A (1994) A. Long-distance neuronal migration in the adult mammalian brain. *Science* **264**, 1145–1148.

Lois C, Garcia-Verdugo JM, Alvarez-Buylla A (1996) Chain migration of neuronal precursors. *Science* **271**, 978–981.

Malatesta P, Hartfuss E, Gotz M (2000) Isolation of radial glial cells by fluorescent-activated cell sorting reveals a neuronal lineage. *Development* **127**, 5253–5263;.

Miyata T, Kawaguchi A, Okano H, Ogawa M (2001) Asymmetric inheritance of radial glial fibers by cortical neurons. *Neuron* **31**, 727–741.

Morimoto T, Ohsawa I, Takamura C, Ishiguro M, Nakamura Y, Kohsaka S (1998a) Novel domain-specific actions of amyloid precursor protein on developing synapses. *J. Neurosci.* **18**, 9386–9393.

Morimoto T, Ohsawa I, Takamura C, Ishiguro M, Kohsaka S (1998b) Involvement of amyloid precursor protein in functional synapse formation in cultured hippocampal neurons. *J. Neurosci. Res.* **51**, 185–195.

Mucke L, Masliah E, Johnson WB, et al. (1994) Synaptotrophic effects of human amyloid beta protein precursors in the cortex of transgenic mice. *Brain Res.* **666**, 151–167.

Noctor SC, Flint AC, Weissman TA, Dammerman RS, Kriegstein AR (2001) Neurons derived from radial glial cells establish radial units in neocortex. *Nature* **409**, 714–720.

Ohsawa I, Takamura C, Kohsaka S (1997) The amino-terminal region of amyloid precursor protein is responsible for neurite outgrowth in rat neocortical explant culture. *Biochem. Biophys. Res. Commun.* **236**, 59–65.

Ohsawa I, Takamura C, Morimoto T, Ishiguro M, Kohsaka S (1999) Amino-terminal region of secreted form of amyloid precursor protein stimulates proliferation of neural stem cells. *Eur. J. Neurosci.* **11**, 1907–1913.

Ohta M, Kitamoto T, Iwaki T, Ohgami T, Fukui M, Tateishi J (1993) Immunohistochemical distribution of amyloid precursor protein during normal rat development. *Brain Res. Dev. Brain Res.* **75**, 151–161.

Ouimet CC, Baerwald KD, Gandy SE, Greengard P (1994) Immunocytochemical localization of amyloid precursor protein in rat brain. *J. Comp. Neurol.* **348**, 244–260.

Palacios G, Palacios JM, Mengod G, Frey P (1992) Beta-amyloid precursor protein localization in the Golgi apparatus in neurons and oligodendrocytes. An immunocytochemical structural and ultrastructural study in normal and axotomized neurons. *Brain Res. Mol. Brain Res.* **15**, 195–206.

Palmer TD, Takahashi J, Gage FH (1997) The adult rat hippocampus contains primordial neural stem cells. *Mol. Cell. Neurosci.* **8**, 389–404.

Peretto P, Merighi A, Fasolo A, Bonfanti L (1997) Glial tubes in the rostral migratory stream of the adult rat. *Brain Res. Bull.* **42**, 9–21.

Peretto P, Merighi A, Fasolo A, Bonfanti L (1999) The subependymal layer in rodents: a site of structural plasticity and cell migration in the adult mammalian brain. *Brain Res. Bull.* **49**, 221–243.

Salbaum JM, Ruddle FH (1994) Embryonic expression pattern of amyloid protein precursor suggests a role in differentiation of specific subsets of neurons. *J. Exp. Zool.* **269**, 116–127.

Sandbrink R, Masters CL, Beyreuther K (1994) Complete nucleotide and deduced amino acid sequence of rat amyloid protein precursor-like protein 2 (APLP2/APPH): two amino acids length difference to human and murine homologues. *Biochem. Biophys. Acta* **1219**, 167–170.

Selkoe DJ (1994) Cell biology of the amyloid beta-protein

precursor and the mechanism of Alzheimer's disease. *Ann. Rev. Cell Biol.* **10**, 373–403.

Seri B, Garcia-Verdugo JM, McEwen BS, Alvarez-Buylla A (2001) Astrocytes give rise to new neurons in the adult mammalian hippocampus. *J. Neurosci.* **21**, 7153–7160.

Sisodia SS, Koo EH, Beyreuther K, Unterbeck A, Price DL (1990) Evidence that beta-amyloid protein in Alzheimer's disease is not derived by normal processing. *Science* **248**, 492–495.

Slunt HH, Thinakaran G, Von Koch C, Lo AC, Tanzi RE, Sisodia SS (1994) Expression of a ubiquitous, cross-reactive homologue of the mouse beta-amyloid precursor protein (APP). *J. Biol. Chem.* **269**, 2637–2744.

Tanzi RE, Gusella JF, Watkins PC, et al. (1987) Amyloid beta protein gene: cDNA, mRNA distribution, and genetic linkage near the Alzheimer locus. *Science* **235**, 880–884.

Trapp BD, Hauer PE (1994) Amyloid precursor protein is enriched in radial glia: implications for neuronal development. *J. Neurosci. Res.* **37**, 538–550.

Wichterle H, Garcia-Verdugo JM, Alvarez-Buylla A (1997) Direct evidence for homotypic, glia-independent neuronal migration. *Neuron* **18**, 779–791.

Zheng H, Jiang M, Trumbauer ME, et al. (1995) Beta-Amyloid precursor protein-deficient mice show reactive gliosis and decreased locomotor activity. *Cell* **81**, 525–531.

GLIA 47:325–334 (2004)

N-myc Downstream-Regulated Gene 1 Expression in Injured Sciatic Nerves

KAZUHO HIRATA,[1]* KATSUAKI MASUDA,[2] WATARU MORIKAWA,[2] JIAN-WEN HE,[1] AKIO KURAOKA,[1] MICHIHIKO KUWANO,[2] AND MASARU KAWABUCHI[1]
[1]*Department of Anatomy and Cell Biology, Graduate School of Medical Sciences, Kyushu University, Fukuoka, Japan*
[2]*Department of Medical Biochemistry, Graduate School of Medical Sciences, Kyushu University, Fukuoka, Japan*

KEY WORDS NDRG1; nerve regeneration; Schwann cells; immunohistochemistry

ABSTRACT N-myc downstream-regulated gene 1 (NDRG1)/RTP/Drg1/Cap43/rit42/TDD5/Ndr1 is expressed ubiquitously and has been proposed to play a role in growth arrest and cell differentiation. A recent study showed that mutation of this gene is responsible for hereditary motor and sensory neuropathy-Lom. However, the role of this gene in the peripheral nervous system is not fully understood. In our study, rabbit polyclonal antibodies were raised against this gene product and were used to examine changes in its expression over the time course of Wallerian degeneration and ensuing regeneration after crush injury of mouse sciatic nerves. Fluorescent immunohistochemistry showed that NDRG1 was expressed over the intact nerve fibers. Double labeling with a Schwann cell (SC) marker, S-100 protein (S-100), revealed that NDRG1 was localized in the cytoplasm of S-100-positive Schwann cells (SCs). NDRG1 expression was maintained in the early stage of myelin degradation but was then markedly depleted at the end stage of myelin degradation when frequent occurrence of BrdU-labeled SCs was observed (at 7–9 days). The depletion of NDRG1 at this time point was also confirmed by Western blotting analysis. NDRG1 expression finally recovered at the stage of remyelination, with immunoreactivity stronger than that in intact nerves. These findings suggest that NDRG1 may play an important role in the terminal differentiation of SCs during nerve regeneration.

INTRODUCTION

N-myc downstream-regulated gene 1 was originally designated reducing agent and tunicamycin-responsive protein (RTP) (Kokame et al., 1996), homologues of which were then isolated repeatedly: human differentiation-related gene 1 (Drg1) (van Belzen et al., 1997), human protein induced by free intracellular Ca^{2+} (Cap43) (Zhou et al., 1998), the mouse homologue designated TDD5 (Lin and Chang, 1997), reduced in tumor, p43 (rit42) (Kurdistani et al., 1998), and N-myc-downstream, repressed gene 1 (Ndr1) (Shimono et al., 1999). Currently the official name of this gene is NDRG1, determined by the HUGO Gene Nomenclature Committee (Qu et al., 2002). We have adopted the nomenclature NDRG1 in this report. A recent study showed that NDRG1 is a member of the NDRG gene family that contains an α/-β-hydrolase fold (Qu et al., 2002) without the residues required for catalysis (Shaw et al., 2002). It encodes a highly conserved protein with a high degree of homology to the proteins in other species, such as zebrafish (Gen Bank Accession Nos. AW281236 and AI657643), fruit flies (AF145604 and AE003454), nematodes (Z68135 and AL132847), sunflowers (Y09057 and AF189147) (Krauter-Canham et al., 1997), and *Arabidopsis* (AC005917 and AL163814). The evolutional conservation of this gene implies that it plays an important biological role. This gene has been reported to be involved in cell growth and differ-

*Correspondence to: Kazuho Hirata, Department of Anatomy and Cell Biology, Graduate School of Medical Sciences, Kyushu University, Higashi-ku, Maidashi 3-1-1, Fukuoka, 812-8582 Japan. E-mail: hirata@anat1.med.kyushu-u.ac.jp

Received 20 September 2003; Accepted 29 January 2004
DOI 10.1002/glia.20037
Published online 30 April 2004 in Wiley InterScience (www.interscience.wiley.com).

entiation (van Belzen et al., 1997; Piquemal et al., 1999; Shimono et al., 1999; Gomez-Casero et al., 2001), stress responses (Kokame et al., 1996; Xu et al., 1999; Agarwala et al., 2000; Salnikow et al., 2000; Segawa et al., 2002), and hormone responses (Lin and Chang, 1997; Ulrix et al., 1999; Segawa et al., 2002). Of particular interest is the observation that NDRG1 may have a complex but important function in carcinogenesis (Guan et al., 2000; Salnikow et al., 2000; Gomez-Casero et al., 2001; Nishie et al., 2001; Segawa et al., 2002; Bandyopadhyay et al., 2003) and atherogenesis (Kokame et al., 1996; Sato et al., 1998). Furthermore, attention has been drawn to the fact that this gene was identified as a gene responsible for hereditary motor and sensory neuropathy-Lom (HMSNL) (Kalaydjieva et al., 2000), which is an autosomal recessive form of Charcot-Marie-Tooth disease (CMT) and an early-onset peripheral neuropathy that progresses to severe disability in adulthood. However, the precise role of NDRG1 in the peripheral nervous system (PNS) remains to be elucidated.

It is well known that after axotomy the PNS has the capacity to be repaired by the established sequential process of Wallerian degeneration and ensuing regeneration (for review, see Hirata and Kawabuchi, 2002). Our previous studies (Hirata et al., 1999; Hirata et al., 2000, 2003) obtained stable and consistent results for the time course of the cellular and molecular events seen in the distal stump of the sciatic nerves following crush injury. It is expected that this crush injury model will provide useful clues for exploring the role of NDRG1 in the PNS. In the present study, polyclonal antibody (pAb) was raised against NDRG1 and was used for immunofluorescent labeling of mouse sciatic nerves after crush injury. The results showed that the expression of NDRG1, which was localized in the cytoplasm of Schwann cells (SCs) in intact nerves, dramatically changed during the process of regeneration. The role of the NDRG1 in the PNS is discussed.

MATERIALS AND METHODS

Production of Polyclonal Anti-NDRG1 Antisera

Synthetic peptides corresponding to internal sequences of human NDRG1 were prepared and used as immunogens. These included the TSEGTRSRSC sequence that corresponds to the tandem repetitive region unique to NDRG1 (Kokame et al., 1996; Okuda and Kondoh, 1999; Shimono et al., 1999). The peptides were coupled with keyhole limpet hemocyanin (KLH) and were used to immunize rabbits.

Immunoblotting Analysis

The sciatic nerves of the intact side and the proximal and distal stumps of the operated side at 9 days after the crush injury were homogenized in 500 ml of 1 mM $NaHCO_3$ buffer (pH 7.2) and centrifuged at 9,000 *g* for 15 min at 4°C. The supernatants were subjected to SDS-PAGE and immunoblotting analysis as described previously (Yamanaka et al., 1997), using a pAb to NDRG1 and peroxidase-conjugated goat anti-rabbit IgG (Jackson, West Grove, PA) diluted at 1:1,000 and 1:10,000, respectively.

TABLE 1. Other Primary Antibodies Used in Immunohistochemical Procedures

Antibody (clone)	Structure/ cell recognized	Source	Dilution	Species
MBP	Myelin	Chemicon	1:100	Rat
NF (NE14)	Axons	Boehringer	1:20	Mouse
S-100	Schwann cells	Bio Makor	1:1000	Mouse
BrdU (biotinylated)	Proliferating cells	Oncogene	Ready-to-use	Mouse
S-100	Schwann cells	Nichirei	1:10	Rabbit

Surgical Procedures

Adult male mice (C57BL6) weighing 20–25 g were used for all experiments. The left sciatic nerve was crushed for 30 s with jeweler's forceps at the mid-thigh level under pentobarbital anesthesia. After the surgery, kanamycin sulfate was sprayed over the entire surgical area and the wound was sutured. The intact contralateral side served as a control. Three mice were sacrificed on each of days 1, 2, 3, 7, 9, 14, and 21 after the operation.

The animals were anesthetized with ether, followed by intracardiac perfusions with 0.01 M phosphate-buffered saline (PBS) and then 4% paraformaldehyde in 0.1 M phosphate buffer (PB). The sciatic nerves were removed at a length of about 6 mm, and consisted of the proximal part (2-mm length), the crush injury site (1-mm length) and the distal part (3-mm length). The segments were postfixed with the same fixative for 3 h and immersed in 15% sucrose in 0.1M PB. They were then embedded in Embedding Matrix and immediately frozen with dry ice and isopentane. Longitudinal and transverse serial sections (10-μm thickness) were cut by using a cryostat microtome.

Immunohistochemistry

The immunohistochemical procedure used in the present study has been described elsewhere (Hirata et al., 2003). Briefly, cryostat sections were fixed again with 100% methanol for 10 min at −20°C and then washed with PBS. Nonspecific binding sites were blocked by preincubation with 1% bovine serum albumin (BSA) or 10% Block Ace (Yukijirushi, Sapporo, Japan) in PBS for 1 h at room temperature (RT). For NDRG1 immunohistochemistry, sections were first incubated with a pAb to NDRG1 diluted 1:100 in PBS overnight at RT and then with fluorescein isothiocya-

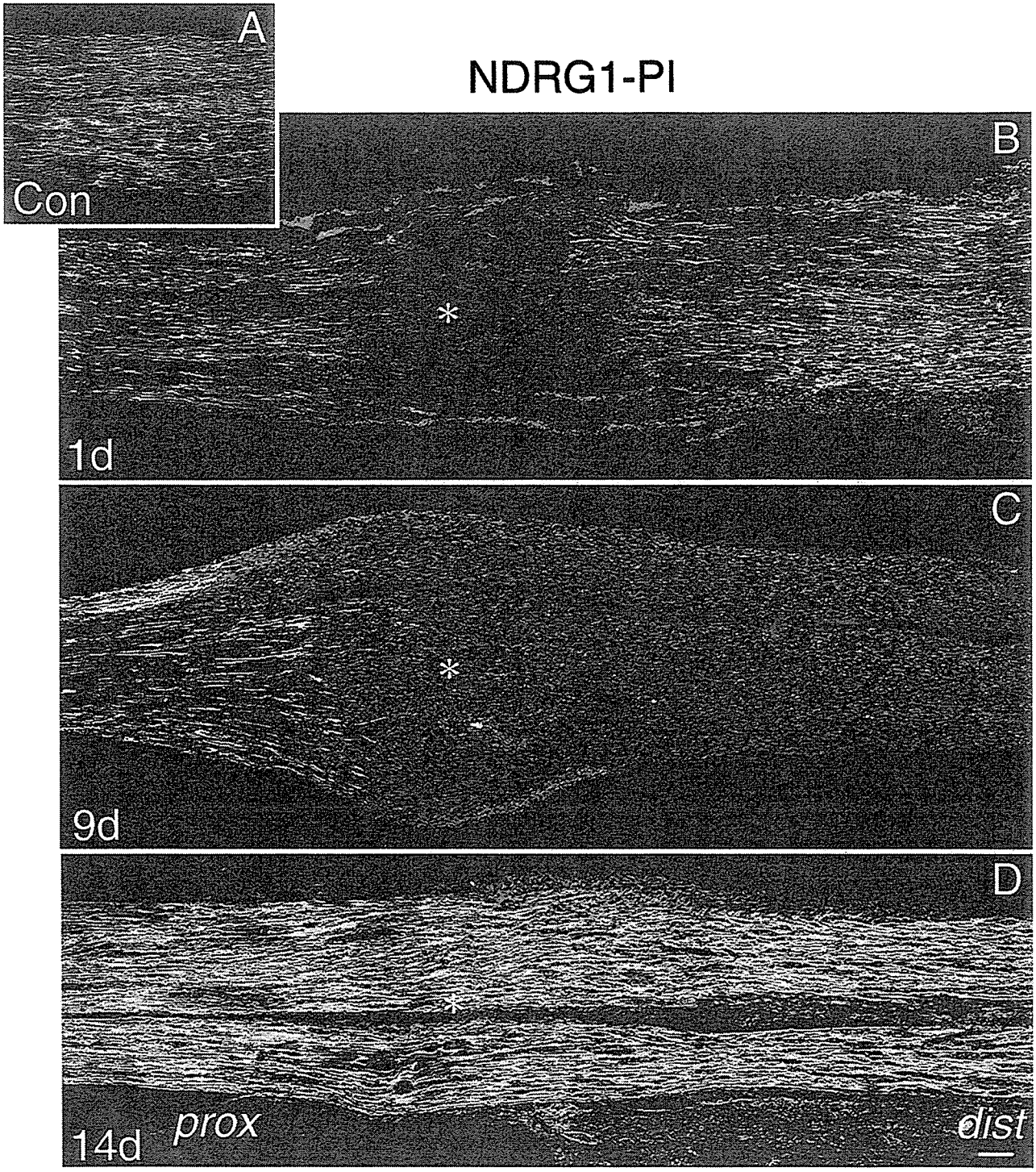

Fig. 1. Expression of NDRG1 (green) in longitudinal sections of intact sciatic nerve used as a control (**A**) and sciatic nerves at 1 day (**B**), 9 days (**C**), and 14 days (**D**) after crush injury. Moderate NDRG1-immunoreactive (-ir) structures seen in the intact nerve (A) remain in the distal stump at 1 day (B), but are hardly detected there at 9 days (C). The NDRG1-ir structures reappear with stronger immunoreactivity than that in the intact nerves at 14 days (D). Asterisks show the crush injury site. The distal and proximal stumps are indicated by dist and prox, respectively. Red indicates nuclei stained by PI. Scale bar = 50 μm

nate (FITC)-conjugated horse anti-rabbit IgG (Vector, Burlingame, CA) for 4 h at room temperature (RT). Control sections were processed identically and in parallel, except that they were incubated with PBS instead of the pAb to NDRG1. No stained cells were seen in these controls. To identify the nuclei of the cells, the

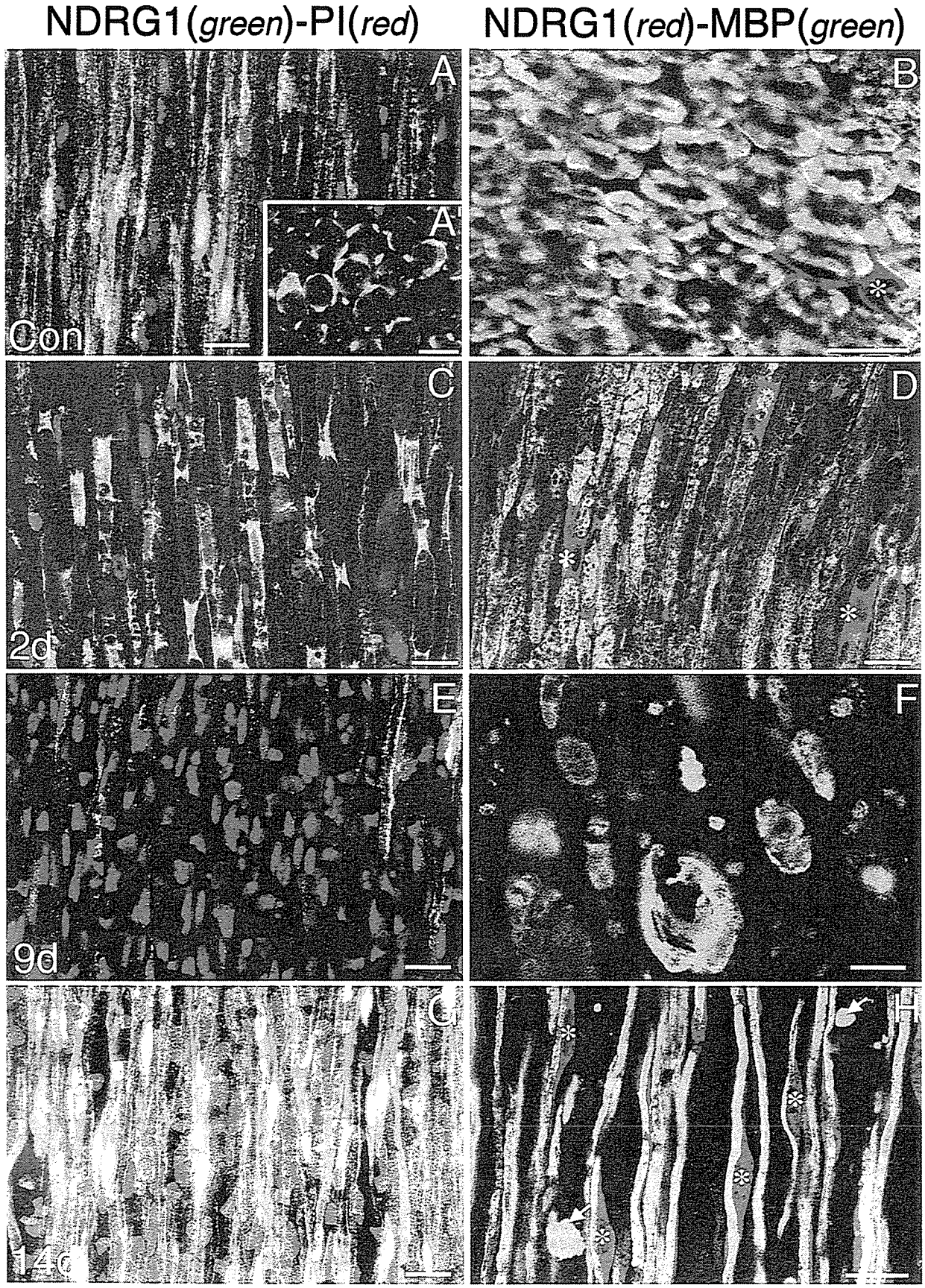
NDRG1(green)-PI(red)
NDRG1(red)-MBP(green)
A
A'
B
Con
C
D
2d
E
F
9d
G
H
14d

Figure 2.

sections were counterstained with propidium iodide (PI) by using a Vectashield mounting medium containing PI (Vector).

To understand the time course of Wallerian degeneration and ensuing regeneration, double immunofluorescent labeling of NDRG1 with a myelin marker (Table 1) was performed. A mixture of a rabbit pAb to NDRG1 and a rat monoclonal antibody (mAb) to myelin basic protein (MBP) was used as the primary antibody. Then, a mixture of Texas red-conjugated donkey anti-rabbit IgG (Jackson) and FITC-conjugated donkey anti-rat IgG (Jackson) was used as the secondary antibody.

Furthermore, double immunofluorescent labeling of NDRG1 with axonal or SC markers (Table 1) was performed. A mixture of a rabbit pAb to NDRG1 and either a mouse mAb to 200-kDa neurofilament protein (NF) or to a mouse mAb to S-100 protein (S-100) was used as the primary antibody. Then, a mixture of FITC-conjugated horse anti-mouse IgG (Vector) and Texas red-conjugated donkey anti-rabbit IgG (Jackson) was used as the secondary antibody. No difference in morphology was noted in any of the immunolabeled structures between the single and double labeling.

To identify mitotic activity of SCs, double immunofluorescent labeling of bromodeoxyuridine (BrdU) and S-100 (Table 1) was performed. Mice were injected intraperitoneally with BrdU (Zymed, CA) (1 ml/100 g) 2 h or 2.5 h prior to being sacrificed. The nerve sections were incubated with a pAb to S-100 as a primary antibody and visualized by Texas red-conjugated donkey anti-rabbit IgG. For subsequent BrdU labeling, part of a BrdU staining kit (Oncogene Research, MA) was used; after treatment with HCl, the biotinylated mouse mAb to BrdU was used as primary antibody. The BrdU binding sites were visualized with streptavidin-FITC (Vector). Double immunofluorescent labeling of NDRG1 and BrdU was attempted, but was unsuccessful since the anti-NDRG1 staining was not compatible with the HCl treatment required for BrdU detection.

Confocal Laser Scanning Microscopy

The sections double-labeled with FITC and PI or FITC and Texas red were scanned with a confocal laser scanning imaging (CLSM) system (LSM-GB200, Olympus, Japan) using excitations at 488 nm (argon laser) for FITC and 568 nm (krypton laser) for PI or Texas red. Single optical sections for each fluorescence were taken separately (channel 1 and channel 2) to avoid any cross-talk and then superimposed. The images were taken using a ×10, ×20, ×40, or ×60 objective lens.

These experiments were reviewed by the Committee on Ethics for Animal Experiments of the Faculty of Medicine, Kyushu University and carried out according to the Guidelines for Animal Experiments of the University, and Law No. 105 and Notification No. 6 of the Japanese government.

RESULTS

In intact sciatic nerves, NDRG1 was expressed over the nerve (Fig. 1A). At 1 day after the crush injury, the expression showed no change except for its disappearance at the injury site (Fig. 1B). At 7–9 days after the crush injury, drastic depletion of the NDRG1 expression was seen at the injury site and the distal stump (Fig. 1C). The expression of NDRG1 then recovered at the injury site and the distal stump at 14 days after the crush injury, showing a slight increase in the immunoreactivity compared to that in the intact nerve (Fig. 1D). Higher magnification of longitudinal (Fig. 2A) and transverse (Fig. 2A′) sections of the intact nerve double-stained with PI nuclear staining showed that NDRG1 immunoreactivity was usually localized in the perinuclear cytoplasm of presumptive SCs of each fiber. Double immunofluorescent labeling with MBP revealed that MBP-immunoreactive (-ir) myelin sheath was usually surrounded by NDRG1-ir cytoplasm (Fig. 2B). At 2 days, cells in the distal stump transformed into cells containing various size of vacuoles, which are known to be characteristic for myelin-phagocytosing cells (Fig. 2C) and double labeling with MBP showed that MBP-ir degraded myelin structures were contained in the vacuoles of NDRG1-ir cells (Fig. 2D). At 7–9 days, NDRG1-ir cells were hardly detected in the injury site (Fig. 2E) and distal stumps (Fig. 2F), where the clearance of myelin debris was considerably progressed (Fig. 2F). At 2 weeks, numerous NDRG1-ir cells with a regular profile similar to that in intact nerves reappeared and the immunoreactivity was stronger than that in the intact nerve (Fig. 2G), and double labeling with MBP revealed that NDRG1-ir cells were in the process of myelinating (Fig. 2H).

Fig. 2. Pseudocolor images of double labeling of NDRG1 (green) with PI (red) (left panel: **A,A′,C,E,G**) and of double immunofluorescent labeling of NDRG1 (red) and MBP (green) (right panel: **B,D,F,H**) of intact nerves (A,A′,B), and of the injury site (E) and the distal stump (C,D,F–H) of crush-injured nerves. All pictures are from longitudinal sections, except for A′,B, which are from transverse sections. Asterisks (B,D,H) indicate sites of nuclei. **A,A′,B:** In intact nerves NDRG1 immunoreactivity is detectable in the perinuclear region of cytoplasm of the presumptive Schwann cells (green in A,A′). **B:** NDRG1-ir cells are myelinating cells, in which MBP-ir myelin sheath (green) are surrounded by a thin layer of NDRG1-ir cytoplasm (red). **C,D:** At 2 days, NDRG1-ir cells (green in C, red in D) have transformed into myelin-phagocytosing cells. D: The vacuoles of the cells seen in C are occupied by MBP-ir degraded myelin structures (green).**E,F:** At 9 days, no clearly stained NDRG1 -ir cells are seen both in the injury site (E) and the distal stump (F). E: Small number of NDRG1 cells seen at the boundary toward the proximal stump (upper). Note that only MBP-ir myelin debris can be seen (green in F). **G,H:** At 14 days, the NDRG1-ir cells reappear showing immunoreactivity stronger (G) than that in the intact nerve (A). H: NDRG1-ir cells are just forming a myelin sheath, judging from the prominent profiles of the perinuclear region (red) and thin MBP-ir myelin sheath (green). Note that strong NDRG1 immunoreactivity is seen not only in the perinuclear region also in the nuclear sites of some cells, suggesting translocation of the protein into nucleus. Arrows indicate the myelin debris. Scale bar = 10 μm.

To identify NDRG1-ir elements, double immunofluorescent labeling with NF, a neuronal marker, or S-100, an SC marker, was carried out. In the cross section of the intact nerve, the NDRG1-ir structure could clearly be distinguished from the NF-ir axons, since the former was localized in the peripheral region of a nerve fiber so that it appeared as a ring-like structure and the latter was in the central part (Fig. 3A). In contrast, the immunoreactive sites of NDRG1 were almost identical with those of S-100 in the intact nerve, suggesting that the NDRG1 was contained only in SCs (Fig. 3B,C). NDRG1 continued to be expressed in S-100-ir SCs, which had the characteristics of myelin-phagocytosing cells at 2 days after the crush injury (Fig.3D,E). At the next stage (7–9 days), the expression of NDRG1 was markedly reduced, whereas the S-100-ir SCs were further transformed to cells with irregular contour (Fig. 3F,G). At the ensuing stage (2 weeks), NDRG1 was reexpressed in S-100-ir SCs, which now showed a regular structure similar to that in the intact nerves.

In the process of nerve regeneration, SCs are known to proliferate following transformation into myelin-phagocytosing cells, and then acquire the immature phenotype to promote axonal regrowth (for review, see Hirata and Kawabuchi, 2002). Double immunofluorescent labeling of BrdU and S-100 was carried out to identify the mitotic activity of SCs. In intact nerves, no cells with BrdU-labeled nuclei were found. At 2 days, only a few S-100-ir SCs with BrdU-labeled nuclei appeared, although presumptive macrophages with BrdU-labeled nuclei were often observed in the perineurium or the epineurium. At 7–9 days (Fig. 4A,C), when the transient depletion of NDRG1 expression occurred, numerous SCs with BrdU-labeled nuclei were detected and distributed throughout the injury site and the distal stump. At 2 weeks, the number of cells with BrdU-labeled nuclei markedly decreased. Thus, the results suggested an inverse relationship between the proliferative activity and NDRG1 expression of SCs. The specificity of BrdU labeling was confirmed in the small intestine (Fig. 4B), where the cells with BrdU-labeled nuclei were specifically distributed in the base of the crypts, known to be the proliferative zone (Potten et al., 1997).

Immunoblotting analysis of sciatic nerves at 9 days after the crush injury revealed that the pAb to NDRG1 labeled a polypeptide band of 43 kDa in the intact nerve (Fig. 5B, lane 1) and the proximal stumps (Fig. 5B, lane 2) but not the distal stumps (Fig. 5B, lane 3) of the crushed nerve. This finding not only confirmed the specificity of the antibody but also indicated preferential depletion of NDRG1 molecules in the injured nerves at this time point. No specific labeling was observed in the control probed with normal rabbit sera.

DISCUSSION

In the present study, immunofluorescent histochemistry and Western blotting analysis using NDRG1 antibodies demonstrated that NDRG1 was expressed in intact mouse sciatic nerve. Double immunofluorescent labeling with an SC marker (S-100) or an axonal marker (NF) showed that NDRG1 was localized in the cytoplasm of SCs, but not in the axons. These findings agree with those of human peripheral nerves analyzed by Northern blotting and RT-PCR (Kalaydjieva et al., 2000) and an immunoenzyme-histochemical technique (Lachat et al., 2002).

Double immunofluorescent labeling of NDRG1 and MBP revealed that NDRG1 was expressed in the cytoplasm of myelinating SCs in intact nerves. Crushed nerves showed little alteration of NDRG1 expression when the myelinating SCs transformed into myelin-phagocytosing cells in the early stage of myelin degradation (Stoll et al., 1989; Hirata et al., 1999). This finding implies that the expression of this protein in SCs is not influenced by either the loss of axonal contact or the transformation of SCs into myelin-phagocytosing cells. Thus, NDRG1 expression does not appear to be regulated during Wallerian degeneration. In contrast, the expression of this protein changed markedly during subsequent process. Both immunohistochemistry and Western blotting analysis demonstrated that NDRG1 expression was dramatically depleted at 7–9 days after the operation, when the myelin removal was considerably progressed. NDRG1 was then reexpressed with more immunoreactivity than that of the intact nerves during remyelination. Thus, our study suggests that NDRG1 may be regulated in the regeneration process of injured nerves.

It is well known that, after taking part in the early stage of myelin removal, SCs proliferate to acquire the immature phenotype and prepare the environments through which regenerating axons grow (for review, see Fawcett and Keynes, 1990; Jessen and Mirsky, 1999; Hirata and Kawabuchi, 2002). In the present study, frequent occurrences of BrdU-labeled SCs were seen at 7–9 days after the crush injury, the timing of which is largely consistent with the occurrence of SC mitosis observed by electron microscopy (O'Daly and Imaeda, 1967). It is noteworthy that the drastic depletion of NDRG1 occurred simultaneously during this period. NDRG1 was reported to be developmentally regulated in embryonic tissues and to be augmented concomitantly with the occurrence of terminal differentiation (Shimono et al., 1999). Direct subtraction of whole mouse embryo cDNAs between the wild type and an N-myc mutant (Shimono et al., 1999) revealed that the NDRG1 gene was repressed by N-myc, a member of the myc family that encodes nuclear phosphoproteins and is believed to play a role in the control of cellular proliferation and differentiation (Melhem et al., 1992). Several lines of in vitro evidence have suggested a role for NDRG1 in cells undergoing terminal differentiation. For example, the NDRG1 gene was upregulated during the differentiation of colon carcinoma cell lines cultured in low glucose medium (van Belzen et al., 1997) and during in vitro forskolin-induced differentiation of a model of the human trophoblast, the chorio-